Quantum-state transfer in staggered coupled-cavity arrays

Guilherme M. A. Almeida,[1,*] Francesco Ciccarello,[2] Tony J. G. Apollaro,[2,3] and Andre M. C. Souza[1]
[1]*Departamento de Física, Universidade Federal de Sergipe, 49100-000 São Cristóvão, Brazil*
[2]*NEST, Istituto Nanoscienze-CNR and Dipartimento di Fisica e Chimica, Università degli Studi di Palermo, via Archirafi 36, I-90123 Palermo, Italy*
[3]*Centre for Theoretical Atomic, Molecular, and Optical Physics, School of Mathematics and Physics, Queen's University Belfast, Belfast BT7 1NN, United Kingdom*
(Received 16 October 2015; revised manuscript received 22 January 2016; published 8 March 2016)

We consider a coupled-cavity array, where each cavity interacts with an atom under the rotating-wave approximation. For a staggered pattern of intercavity couplings, a pair of field normal modes, each bilocalized at the two array ends, arises. A rich structure of dynamical regimes can hence be addressed, depending on which resonance condition is set between the atom and the field modes. We show that this can be harnessed to carry out high-fidelity quantum-state transfer (QST) of photonic, atomic, or polaritonic states. Moreover, by partitioning the array into coupled modules of shorter length, the QST time can be substantially shortened without significantly affecting the fidelity.

DOI: 10.1103/PhysRevA.93.032310

I. INTRODUCTION

The potential of coupled high-quality cavities as a platform for simulating many-body quantum phenomena has attracted considerable interest over the past few years [1,2]. Such an architecture would indeed enable a high degree of control and addressability of individual sites. Moreover, the coupling to atoms results in the formation of polaritons (pseudoparticles involving atomic and photonic excitations), which can give rise to novel strongly correlated regimes of light and matter.

A prototype of such systems is a coupled-cavity array (CCA) described by the so-called Jaynes-Cummings-Hubbard (JCH) model [3,4], where—due to the overlap between evanescent field modes—photons can hop across nearest-neighbor cavities and, at the same time, interact with two-level quantum emitters ("atoms"). In the strong atom-field coupling regime, an effective repulsive photon-photon interaction takes place, resulting in a Mott-insulator state for the system [3–12]. The competition between this photon-blockade effect [13] and the photon hopping creates a Mott-insulator–superfluid quantum phase transition in analogy with the Bose-Hubbard model [14].

Besides being promising quantum simulators (cf. Ref. [15] for a recent implementation of a Jaynes-Cummings (JC) dimer in a superconducting circuit), coupled-cavity networks are attractive platforms for distributed quantum information processing and quantum communication [16–18]. Among its crucial requirements, a quantum network must be capable of creating entanglement, performing quantum gates, and transmitting quantum states between arbitrarily distant nodes. As atomic systems are long-lived quantum memories and photons can faithfully carry information over long distances, hybrid atom-photon interfaces indeed appear to be ideal building blocks of a quantum network architecture [19,20].

From this perspective, a key issue is the study of excitation transport—in the form of photonic, atomic, or polaritonic excitations—as well as quantum-state transfer (QST) [21,22] across CCAs [23–35]. Nontrivial dynamics are also exhibited by CCAs featuring only a single cavity coupled to an atom [36–41].

In this paper, we explore the potential of a CCA to work as a bus for achieving high-fidelity QST without demanding any dynamical control or measurement. QST is a pivotal task in quantum communication, which has been intensively investigated, mostly in connection with spin chains following the seminal proposal by Bose [21] (for a review see, e.g., Ref. [22]). Given an array of coupled qubits (such as a spin chain), the goal of QST is transferring an arbitrary quantum state of a qubit located at one end of the array to the qubit at the opposite end. This should be performed by simply letting the many-qubit system evolve in time according to its Hamiltonian. Achieving this with a high efficiency is, in general, nontrivial. For instance, this is not possible in chains (especially long ones) with uniform spin-spin couplings [21] due to the detrimental dispersion of the initial wave packet. To get around it, several schemes were thus put forward. It was shown, in particular, that perfect length-independent QST can be reached by engineering the spin-spin couplings so as to induce a linear dispersion relation [42,43]. This yields a ballistic QST, entailing that the QST time is proportional to the chain length. A reliable local modulation involving the entire chain, however, would face several practical difficulties on the experimental side. Ballistic QST can also be achieved under appropriate tuning of the outermost couplings [44,45]. A different approach relies on the weak interaction of the sender and receiver spins with a bulk embodied by a uniform chain [46,47]. Schemes of this kind exploit the appearance of a pair of Hamiltonian eigenstates strongly bilocalized at the outermost weakly coupled sites (behaving as chain defects), which brings about an effective Rabi-like dynamics [46]. A similar dynamics can be triggered by applying strong magnetic fields to the sender and receiver qubits or their nearest neighbors [48–50]. At variance with ballistic QST protocols, a usual drawback of Rabi-like mechanisms is that they typically require long QST times.

Here, we assume a scheme of staggered intercavity coupling strengths, also known as the Peierls distorted chain [51], which has been addressed for QST [52,53] and quantum teleportation

*gmaalmeidaphys@gmail.com

protocols [54–56] in spin systems (CCAs were considered for implementing distorted chains in Refs. [55,56]). This model also belongs to the class of QST schemes relying on Rabi-like dynamics, hence requiring relatively long transfer times. One of our goals is to keep a high-quality QST via Rabi-like dynamics but, at the same time, significantly reduce the required transfer time. We show that this can be achieved by *modularizing* the array, namely, connecting identical subunits of Peierls distorted chains. We first discuss this in detail for an atom-free CCA, which also applies to any spin chain (irrespective of its realization) having an analogous pattern of couplings. We then show how to exploit these findings when the CCA is coupled to atoms in order to devise schemes for transferring atomic or polaritonic states.

The present paper is organized as follows. In Sec. II, we study the single-photon spectrum and stationary states of a staggered CCA, highlighting, in particular, the features that are crucial for QST purposes. In Sec. III, we review the basic ideas of QST in spin chains, with a special focus on those schemes whose working principle relies on the formation of bilocalized states. In Sec. IV, we study QST across a staggered atom-free CCA. In Sec. V, we show how the staggered CCA can be modified so as to shorten the QST transfer time. In Sec. VI, we study the CCA dynamics in the presence of atoms and the regimes that are relevant for QST. In Sec. VII, we show how to achieve QST of atomic and polaritonic qubits. Finally, in Sec. VIII we draw our conclusions.

II. CCA WITH STAGGERED HOPPING RATES

Our setup consists of a CCA comprising an *even* number N of identical, single-mode, lossless cavities. Nearest-neighbor cavities are coupled according to a staggered pattern of hopping rates such that two possible hopping rates J_1 and J_2 are interspersed along the array, as sketched in Fig. 1. Each cavity in turn (see Fig. 1) can be coupled to a two-level quantum emitter (atom).

In this and the following three sections, we focus on the free-field Hamiltonian, i.e., that of an atom-free CCA. We consider the full setup, including the atoms, starting in Sec. VI.

The free-field Hamiltonian of the staggered CCA is modeled as (we set $\hbar = 1$ throughout)

$$\hat{H}_{\rm hop} = -J \sum_{x=1}^{N-1} [1-(-1)^x \eta]\, (\hat{a}_{x+1}^\dagger \hat{a}_x + \text{H.c.}), \qquad (1)$$

where the bosonic ladder operator $\hat{a}_x^\dagger$ ($\hat{a}_x$) creates (annihilates) a photon at the xth cavity. Note that for odd (even) x the quantity in brackets in Eq. (1) equals $J_1 = (1+\eta)J$ [$J_2 = (1-\eta)J$], where J sets the hopping scale and $-1 \leqslant \eta \leqslant 1$ is a dimensionless distortion parameter (rates are always expressed in units of J). For $\eta = 0$, we retrieve the CCA with uniform intercavity couplings usually considered in JCH models [27]. We also point out that, since N is even, for $\eta \to -1^+$ the two outermost cavities (corresponding to $x = 1$ and $x = N$, respectively) are weakly coupled to the remaining ones (bulk), a property which is crucial for our goals. In assuming that the free-field Hamiltonian is given by Eq. (1), we have neglected the usual on-site contribution $\sum_x \omega_c\, \hat{a}_x^\dagger \hat{a}_x$, with ω_c being the frequency of the each cavity-protected mode, which is equivalent to setting the energy scale such that $\omega_c = 0$.

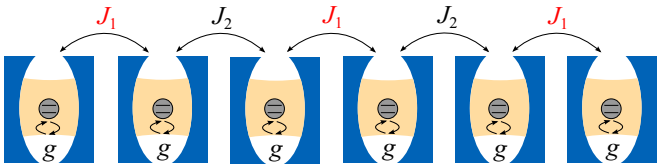

FIG. 1. Sketch of a CCA with a staggered pattern of hopping rates, where $J_1 = (1+\eta)J$ and $J_2 = (1-\eta)J$. The protected mode of each cavity can be coupled to a two-level atom at rate g.

Our first task is to diagonalize Hamiltonian (1) in the single-photon Hilbert space, which is spanned by the basis $\{|x\rangle\}$, with $|x\rangle = \hat{a}_x^\dagger|\text{vac}\rangle$ and $|\text{vac}\rangle$ being the field vacuum state. Recalling that N is even, Hamiltonian $\hat{H}_{\rm hop}$ evidently enjoys a mirror symmetry with respect to its middle point; i.e., it is invariant under the transformation $\hat{P}|x\rangle = |N-x+1\rangle$, where $\hat{P}$ is the parity operator. Thereby, $\hat{H}_{\rm hop}$ can be block-diagonalized, each block corresponding to a subspace of a given parity (even or odd). The even (odd) subspace is $N/2$-dimensional and spanned by the basis $\{|x\rangle_+\}$ ($\{|x\rangle_-\}$) with $|x\rangle_\pm = (|x\rangle \pm |N-x+1\rangle)/\sqrt{2}$, where x runs from 1 to $N/2$. For now, we add the requirement that the number of cavities is such that $N/2$ must be odd, which is equivalent to demanding that N—besides being even—is not an integer multiple of 4 (for our purposes, this is only a mild restriction).

It is straightforward to check that the parity subspaces introduced above yield an effective representation of Hamiltonian (1) given by

$$\hat{H}_{\rm hop}^{(\pm)} = -J \sum_{x=1}^{N/2-1} [1-(-1)^x \eta]\, (\hat{a}_{x+1}^{(\pm)\dagger} \hat{a}_x^{(\pm)} + \text{H.c.}) \mp J_1 \hat{a}_{N/2}^{(\pm)\dagger} \hat{a}_{N/2}^{(\pm)}, \qquad (2)$$

with $\hat{a}^{(\pm)\dagger}|\text{vac}\rangle = |x\rangle_\pm$ (if $N/2$ is even, an analogous expression holds, but replacing $J_1 \to J_2$ in the last term). Note that, unlike in Fig. 1 where the outermost couplings are equal to J_1, here the leftmost and rightmost couplings are J_1 and J_2, respectively. Thus, Hamiltonian $\hat{H}_{\rm hop}^{(\pm)}$ describes an effective array comprising an *odd* number of cavities featuring a staggered pattern of hopping rates and a defect at the rightmost cavity $x = N/2$. This defect consists in a local-frequency shift $\mp J_1$.

For convenience, let us define $M = N/2$ and $\hat{V}_\pm = \mp J_1 \hat{a}_M^{(\pm)\dagger} \hat{a}_M^{(\pm)}$, where the latter describes the defect term in Eq. (2). We can now tackle the problem perturbatively by interpreting $\hat{V}_\pm$ as a perturbation in a defect-free staggered CCA consisting of an odd number of cavities, a model which can be exactly solved in the single-excitation subspace [29].

A. Diagonalization of $\hat{H}_{\rm hop}^{(\pm)}$ for $\hat{V}_\pm = 0$

Based on Ref. [29], for $\hat{V}_\pm = 0$ (no defect) the spectrum of $\hat{H}_{\rm hop}^{(\pm)}$ comprises a pair of bands (separated by a gap $\Delta\omega$)

alongside a discrete frequency $\omega_b = 0$ falling in the middle of the gap. The latter corresponds to a bound eigenstate $|\alpha_b\rangle$, which is localized in the vicinity of only one of the array edges (which of the two depends on the sign of η). This reads

$$|\alpha_b\rangle = \mathcal{C}\sum_{x=1}^{\frac{M+1}{2}} \mathcal{D}^{x-1}|2x-1\rangle_{\pm}, \tag{3}$$

with

$$\mathcal{D} = \frac{J_1}{J_2} = \frac{1+\eta}{1-\eta}, \quad \mathcal{C} = \frac{2}{\eta-1}\sqrt{\frac{\eta}{\mathcal{D}^{M+1}-1}}, \tag{4}$$

where $\mathcal{D}$ can be interpreted as the distortion ratio. Note that the spatial amplitude of the bound mode, ${}_{\pm}\langle x|\alpha_b\rangle$, decays exponentially as x moves away from the weakly coupled edge. Also, ${}_{\pm}\langle x|\alpha_b\rangle = 0$ for even $|x\rangle_{\pm}$.

All the remaining eigenvalues, instead, are given by $\omega_{k\mu} = -\mu E_k$, with $\mu = \pm$ (band index) and

$$E_k = 2J\sqrt{\cos^2\frac{k}{2} + \eta^2\sin^2\frac{k}{2}}, \tag{5}$$

where $k = 2\pi j/(M+1)$ for $j = 1,2,\ldots,(M-1)/2$. These describe a pair of energy bands separated by a band gap $\Delta\omega \leqslant 4J$, with the identity holding only when $|\eta| = 1$ The eigenstates corresponding to $\omega_{k\mu}$ are worked out as [29]

$$|\alpha_{k\mu}\rangle = \sqrt{\frac{2}{M+1}}\left(\sum_{x=1}^{\frac{M-1}{2}}\sin(kx)|2x\rangle_{\pm} + \mu\sum_{x=1}^{\frac{M+1}{2}}\sin(kx+\vartheta_k)|2x-1\rangle_{\pm}\right), \tag{6}$$

where the phase ϑ_k is defined by the identity $e^{i\vartheta_k} = J(1-\eta)(e^{-ik}-\mathcal{D})/E_k$.

B. Peturbative diagonalization of $\hat{H}^{(\pm)}_{\rm hop}$

Let us now tackle the full problem of diagonalizing $\hat{H}^{\pm}_{\rm hop}$ (taking the defect into account). If $J_1 \ll J_2$, meaning that the end cavities are weakly coupled to the bulk (see Fig. 1), $\hat{V}_{\pm}$ can be treated as a small perturbation. Applying standard first-order perturbation theory, the bound-mode frequency $\omega_b = 0$ is then straightforwardly corrected as

$$\omega_{b_\pm} \simeq \omega_b \mp J_1\langle\alpha_b|\hat{a}_M^{(\pm)\dagger}\hat{a}_M^{(\pm)}|\alpha_b\rangle = \mp\frac{4J\eta\mathcal{D}^M}{(\eta-1)(\mathcal{D}^{M+1}-1)}, \tag{7}$$

where terms $\sim O(J_1^2)$ have been neglected. The perturbation thereby splits ω_b into two discrete frequencies separated by the energy gap

$$\delta\omega = \omega_{b_-} - \omega_{b+} = \frac{8J\eta}{\eta-1}\,\frac{\left(\frac{1+\eta}{1-\eta}\right)^{N/2}}{\left(\frac{1+\eta}{1-\eta}\right)^{N/2+1}-1}, \tag{8}$$

where we have used Eqs. (4) and (7) and replaced $M = N/2$.

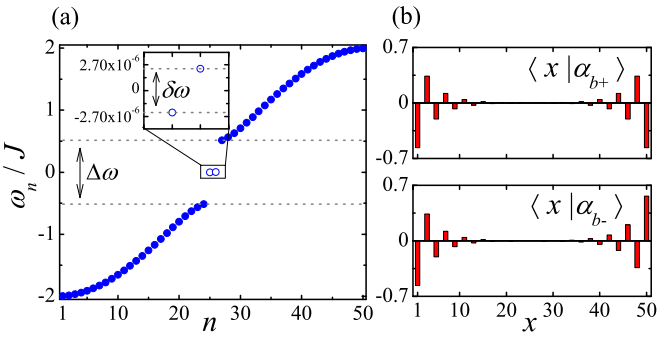

FIG. 2. (a) Single-excitation spectrum of Hamiltonian (1) (in units of J). $\Delta\omega$ is the gap between the pair of bands corresponding to unbound states, while $\delta\omega = \omega_{b_-} - \omega_{b+}$ (inset) is the energy gap between the localized bound states [cf. Eq. (8)]. (b) Spatial profile of $|\alpha_{b\pm}\rangle$. Plots were obtained by exact numerical diagonalization of Eq. (1) for $\eta = -0.25$ and $N = 50$ [comparison with perturbation theory, Eqs. (7) and (9), is found to be excellent].

The corresponding eigenstates are evaluated as

$$|\alpha_{b_\pm}\rangle \simeq |\alpha_b\rangle \mp J_1\sum_{k,\mu}\frac{\langle\alpha_{k\mu}|\hat{a}_M^\dagger\hat{a}_M|\alpha_b\rangle}{\omega_b-\omega_{k\mu}}|\alpha_{k\mu}\rangle$$
$$= |\alpha_b\rangle \mp 4J\mathcal{C}\left(\frac{\eta+1}{M+1}\right)\mathcal{D}^{\frac{M-1}{2}}\sum_k\sum_{x=1}^{\frac{M-1}{2}}\frac{\sin(kx)}{E_k} \times \sin\left[\left(\frac{M+1}{2}\right)k+\vartheta_k\right]|2x\rangle_{\pm}. \tag{9}$$

The unbound states of $\hat{H}^{(\pm)}_{\rm hop}$ can be easily obtained as well, though they yield extensive expressions, which we do not report here for the sake of brevity. In Fig. 2, we consider the paradigmatic instance $\eta = -0.25$ and $N = 50$ and display the energy spectrum of the full Hamiltonian, (1), alongside the spatial profile of the bound states, (9), on the actual array (i.e., in the basis $\{|x\rangle\}$). We see that the two localized bound states are well isolated from the unbound modes (the latter corresponding to the pair of bands). They exhibit an energy splitting $\delta\omega$ that, although negligible compared to the band gap $\Delta\omega$, is nonzero. Moreover, each bound state is strongly localized in the vicinity of the array edges (i.e., cavities $x = 1$ and $x = N$), a property which henceforth we refer to as *bilocalization*. These features are key sources for performing QST, as we discuss next.

III. QUANTUM-STATE TRANSFER: REVIEW

QST protocols are typically formulated in one-dimensional XX-type spin chains, which can be described in terms of ladder spin operators yielding a Hamiltonian of the general form

$$\hat{H}_{\rm ch} = \sum_{x=1}^{N} B_x\hat{\sigma}_x^+\hat{\sigma}_x^- + \sum_{x=1}^{N-1} J_x(\hat{\sigma}_{x+1}^+\hat{\sigma}_x^- + \text{H.c.}), \tag{10}$$

where B_x is a local effective magnetic field and $\hat{\sigma}_x^+ = [\hat{\sigma}_x^-]^\dagger = |1\rangle_x\langle 0|$, with $\{|0\rangle_x, |1\rangle_x\}$ being a single-spin orthonormal basis. Note that Hamiltonian (10) conserves the total number of excitations, i.e., $[\sum_x \hat{\sigma}_x^+\hat{\sigma}_x^-, \hat{H}_{\rm ch}] = 0$. In the single-excitation

subspace, the Hamiltonian reduces to a tridiagonal matrix describing a standard hopping model.

A. Basics of QST

In the usual QST scheme [21], the sender prepares an arbitrary qubit state $|\phi\rangle_1 = c_0|0\rangle_1 + c_1|1\rangle_1$ at the first site and sets the rest of the chain to $|0\rangle_2 \ldots |0\rangle_N$. The initial state of the whole chain thus reads $|\Psi(0)\rangle = |\phi\rangle_1|0\rangle_2 \ldots |0\rangle_N$. The system then evolves according to its Hamiltonian $\hat{H}_{\rm ch}$ so that at time t its state is given by $|\Psi(t)\rangle = \hat{U}(t)|\Psi(0)\rangle$ with $\hat{U}(t) = e^{-i\hat{H}_{\rm ch}t}$. The goal is to exploit such natural dynamics to transfer the initial sender's state $|\phi\rangle$ to the Nth spin (receiver) in a given time τ, meaning that $|\Psi(\tau)\rangle = |0\rangle_1 \ldots |0\rangle_{N-1}|\phi\rangle_N$. The received (generally mixed) state is evaluated by tracing out the remaining spins, i.e., $\rho_N(\tau) = {\rm Tr}_{1,\ldots,N-1}|\Psi(\tau)\rangle\langle\Psi(\tau)|$. One thus aims at making the QST fidelity $F_\phi(\tau) = \langle\phi|\rho_N(\tau)|\phi\rangle$ as large as possible (the fidelity F_ϕ measures how close the receiver's state is to $|\phi\rangle$).

The fidelity introduced above depends on the specific input $|\phi\rangle$. In order to end up with a state-independent figure of merit for QST, one needs to average F_ϕ over all possible input states on the Bloch sphere ($|c_0|^2 + |c_1|^2 = 1$). For Hamiltonians of the form of (10), which conserves the total number of excitations, and given that $|\Psi(0)\rangle$ is restricted to evolving in the zero- and one-excitation subspaces, the former being unaffected by $U(t)$, the *average fidelity* is simply given by [21]

$$\mathcal{F}(t) = \frac{1}{2} + \frac{|f(t)|}{3} + \frac{|f(t)|^2}{6}, \tag{11}$$

where

$$f(t) = \langle N|e^{-i\hat{H}_{\rm ch}t}|1\rangle \tag{12}$$

is the excitation transition amplitude from the first to the last spin. (We used the compact notation $|x\rangle \equiv \hat{\sigma}_x^+|0\rangle_1 \ldots |0\rangle_N$.) Note that $|f(\tau)| = 1$ entails $\mathcal{F}(\tau) = 1$ (perfect QST). Also, the average fidelity is a monotonic function of the transition amplitude and hence the QST performance can be evaluated by just tracking down the excitation transport across the array.

When the state to be transferred is encoded in more than two levels (a qutrit for instance) and/or the chain is not properly initialized (thus containing unwanted excitations), the average fidelity is not expressed by Eq. (11), even though it still depends on the involved transition amplitudes [34,57].

B. Rabi-like QST

In the single-excitation sector, the spectral decomposition of Hamiltonian (10) reads $\hat{H}_{\rm ch} = \sum_{j=1}^N \omega_j|\upsilon_j\rangle\langle\upsilon_j|$, where ω_j is the jth energy eigenvalue with corresponding eigenstate $|\upsilon_j\rangle = \sum_{j=1}^N \upsilon_{jx}|x\rangle$. In this representation, the transition amplitude discussed above is given by

$$f(t) = \sum_{j=1}^N e^{-i\omega_j t}\upsilon_{jN}^*\upsilon_{j1} = \sum_{j=1}^N e^{-i\omega_j t}\langle\upsilon_j|\hat{\sigma}_1^+\hat{\sigma}_N^-|\upsilon_j\rangle. \tag{13}$$

The last identity shows that each eigenstate contributes to Eq. (13) through the quantity $\langle\upsilon_j|\hat{\sigma}_1^+\hat{\sigma}_N^-|\upsilon_j\rangle$, evolving in time at rate ω_j. In the remainder of this paper, we refer to it as the *end-to-end amplitude*.

Various high-quality QST schemes [46,48,49,52,58] rely on the situation where the edge states $|1\rangle$ and $|N\rangle$ have a strong overlap with only two stationary states, say those indexed by $j = 1,2$ (bilocalization). In this case, Eq. (13) can be approximated as

$$f(t) \simeq e^{-i\frac{\delta\omega t}{2}}\langle\upsilon_1|\hat{\sigma}_1^+\hat{\sigma}_N^-|\upsilon_1\rangle + e^{i\frac{\delta\omega t}{2}}\langle\upsilon_2|\hat{\sigma}_1^+\hat{\sigma}_N^-|\upsilon_2\rangle \tag{14}$$

with $\delta\omega = \omega_1 - \omega_2$ (we have assumed $\omega_1 > \omega_2$). This entails a Rabi-like dynamics that occurs with a characteristic Rabi frequency given by $\delta\omega$. Accordingly, $\tau \sim \delta\omega^{-1}$, showing that the order of magnitude of the transmission time is set by the energy gap between the two bilocalized eigenstates.

The above bilocalization effect is usually achieved by introducing perturbation terms in the Hamiltonian that decouple the outermost spins from the bulk. This can be realized (i) by applying strong local magnetic fields on the edge spins [48,58], (ii) by applying such fields on their nearest-neighbors [49], and (iii) by engineering weak couplings between the edge spins and the bulk [46,52]. While all these models share that a pair of Hamiltonian eigenstates exhibits strong bilocalizaton at the edge sites, the typical energy gap between such two states—and, accordingly, the transmission time—depend on the considered model. Calling ξ the model-dependent perturbation parameter (such as the local magnetic field strength), for (i) the time scales with N as $\tau \sim \xi^N$, resulting in a QST time that increases exponentially with the array length, whereas for (ii) and (iii) the time scales as $O(\xi^2)$ and $O(\xi^{-2})$, respectively. All these typical transfer times are, in general, relatively long and may easily exceed the system's coherence time scale. Therefore, it is of great importance to design protocols requiring shorter transfer times.

IV. QST IN AN ATOM-FREE STAGGERED CCA

Comparing Eqs. (1) and (10), it should be evident that within the single-excitation subspace, one can regard the spin chain as an atom-free CCA. Indeed, in this case the mapping is straightforward and reads $\hat{\sigma}_x^+ \to \hat{a}_x^\dagger$, $\hat{\sigma}_x^- \to \hat{a}_x$. Likewise, the QST protocol discussed in Sec. III A now takes place in the zero- and one-photon sectors $\{|{\rm vac}\rangle, |x\rangle\}$. Until Sec. V we thus address QST along a staggered CCA with no atoms. This will introduce one of our main results in Sec. V, where we show that the staggered CCA QST time can be significantly reduced by adding *modularization* on top of the staggered scheme. On the one hand, this analysis provides the necessary basis for QST on CCAs coupled to atoms, which we investigate starting in Sec. VI. On the other hand, it has its own relevance since our findings are independent of the CCA-based implementation, hence they apply to any spin chain with an analogous pattern of couplings.

In the light of Secs. II and III, the atom-free staggered array is suitable for implementing QST based on bilocalization (see Sec. III B) in the regime $J_1 \ll J_2$. To see this, consider first the limiting case $J_1 = 0$, i.e., $\eta = -1$. In this limit (dimerization), the array reduces to a pair of isolated cavities at the outermost sites and a bulk of uncoupled dimers [see the inset sketch at the top in Fig. 3(a)]. The pair of bound states [cf. Eq. (9)] then reduces to the doublet $|\alpha_{b\pm}\rangle = (|1\rangle \pm |N\rangle)/\sqrt{2}$ with $\omega_{b_\pm} = 0$, these evidently being the only stationary states with nonzero

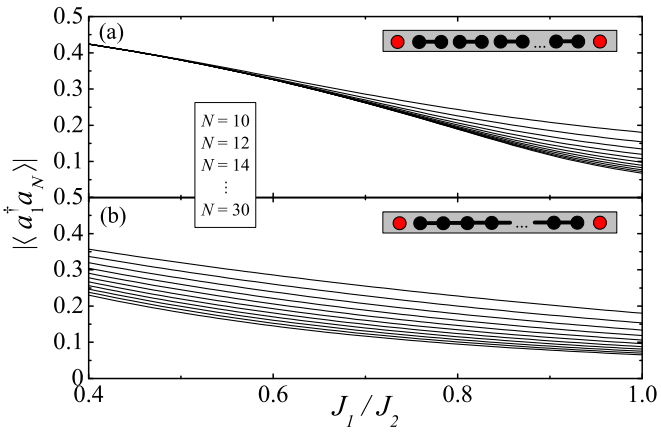

FIG. 3. End-to-end amplitude $|\langle\alpha_{b\pm}|\hat{a}_1^\dagger\hat{a}_N|\alpha_{b\pm}\rangle|$ vs J_1/J_2 for several values of N (in increasing order from top to bottom) in the case of (a) a staggered array described by Hamiltonian (1) and (b) a uniform bulk described by Hamiltonian (17). Note that J_1/J_2 decreases from right to left. Each plot was obtained from an exact numerical diagonalization of the Hamiltonian.

amplitude at the array ends. This would turn Eq. (14) into an exact identity, with $\{|\alpha_{b\pm}\rangle\}$ embodying the pair $\{|\upsilon_1\rangle,|\upsilon_2\rangle\}$. Yet, due to $\omega_{b_\pm}=0$, the transmission time τ would be infinite since $\delta\omega=0$. To make this finite, we thus need to work in the regime $J_1\ll J_2$, which justifies our perturbative approach in Sec. II B.

Next, with the help of Eqs. (3) and (9), we note that the end-to-end amplitudes entering Eq. (14) fulfill

$$\langle\alpha_{b\pm}|\hat{a}_1^\dagger\hat{a}_N|\alpha_{b\pm}\rangle=\pm\tfrac{\mathcal{C}^2}{2}+O\big(J_1^2\big). \tag{15}$$

Thereby, the transition amplitude's modulus reads

$$|f(t)|=2\left|\langle\hat{a}_1^\dagger\hat{a}_N\rangle\sin\left(\frac{\delta\omega}{2}t\right)\right|, \tag{16}$$

where $\langle\hat{a}_1^\dagger\hat{a}_N\rangle$ is short notation for the end-to-end amplitude. At times $t=2n\pi/\delta\omega$, with n being an odd integer, Eq. (16) reaches the value $2|\langle\hat{a}_1^\dagger\hat{a}_N\rangle|$. Hence, ideally, if the absolute value of the end-to-end amplitude equals $1/2$, perfect QST is attained with transmission time $\tau=2\pi/\delta\omega$.

In Fig. 3(a), based on exact numerical diagonalization of Eq. (1), we explore how the end-to-end amplitude is affected by the array size N and J_1/J_2. For a set ratio J_1/J_2, the amplitude decreases with N, eventually saturating to an asymptotic value. For $J_1/J_2=1$ (uniform hopping rates) the asymptotic value is well below $1/2$ but tends to it as J_1/J_2 approaches 0. At the same time, remarkably, the rapidity at which $|\langle\hat{a}_1^\dagger\hat{a}_N\rangle|$ saturates to such an asymptotic value as a function of N increases in a way that, for J_1/J_2 small enough, the amplitude becomes in fact N independent. This agrees with Eq. (15) [see also Eq. (4)].

In other words, for a very distorted array, the bilocalization effect required for high-fidelity QST is almost insensitive to the system size. This property is related to what is known as true long-distance entanglement exhibited by the ground state of staggered spin chains [54], as opposed to quasi-long-distance entanglement featuring quantum correlations that decrease with N. The latter occurs, for instance, in spin chains comprising a uniform bulk [46,54]. The fundamentally different nature of those two situations is reflected in the scaling properties of QST fidelity as well. To show this, consider a CCA where—unlike the staggered array—the bulk cavities are coupled uniformly with rate J_2 [see inset sketch at the top in Fig. 3(b)]. The Hamiltonian of such an array thus reads

$$\hat{H}'_{\rm hop}=-J_1(\hat{a}_2^\dagger\hat{a}_1+\hat{a}_N^\dagger\hat{a}_{N-1})-J_2\sum_{x=2}^{N-2}\hat{a}_{x+1}^\dagger\hat{a}_x+\text{H.c.} \tag{17}$$

Since the outermost sites are weakly coupled to the bulk, a pair of bilocalized eigenstates is formed in this case too [46]. In Fig. 3(b), we plot the corresponding end-to-end amplitude as a function of J_1/J_2 and N. The differences with respect to the staggered-CCA case are quite striking. While for $J_1/J_2=1$ (fully uniform array) both models coincide, the end-to-end amplitude in the uniform-bulk case decreases with N, at variance with the stable behavior found in the staggered model, taking, moreover, lower values compared to the latter. This shows some of the attractive features of staggered arrays in terms of QST fidelity.

V. MODULARIZED ARRAY

The advantages highlighted in the previous section, however, come with a price in terms of the transmission time τ required for carrying out QST. Recalling that $\tau\sim\delta\omega^{-1}$, Eq. (8) indeed shows that, in the regime $J_1\ll J_2$ (i.e., $\eta\simeq-1$), the bound-state gap $\delta\omega$ exponentially decays with the size N. As a consequence, τ exponentially increases with N. One thus wonders whether, for a given size, the staggered array can be modified so as to increase the gap while maintaining the bilocalization strength of $|\alpha_{b\pm}\rangle$ (necessary to attain high fidelity). In this section, we show that this can be achieved by modularizing the staggered CCA.

The setup we put forward is inspired by the concept of modular entanglement introduced in Ref. [59]. Let us consider then a set of m identical staggered arrays, having N sites each, so that the total number of sites is $L=mN$. Nearest-neighbor cavities of adjacent modules are coupled with hopping rate $J_{\rm mod}$, hence the total Hamiltonian reads

$$\hat{H}_{\rm mod}=\sum_{j=1}^{m}\hat{H}_{\rm hop}^{(j)}-J_{\rm mod}\sum_{j=1}^{m-1}(\hat{a}_{jN+1}^\dagger\hat{a}_{jN}+\text{H.c.}), \tag{18}$$

where the free module Hamiltonian $\hat{H}_{\rm hop}^{(j)}$ is the same as Eq. (1) [the sum now being over $x=(j-1)N+1,jN-1$].

For $J_{\rm mod}=J_2$, the whole setup reduces to a standard staggered array comprising L cavities. In contrast, in the limit $J_{\rm mod}=0$ (no intermodular couplings), the energy spectrum and associated eigenstates of $\hat{H}_{\rm mod}$ are the same as those of the single N-long module analyzed in Sec. II, but becoming m-fold degenerate. For intermediate values $0<J_{\rm mod}<J_2$, this degeneracy is removed, resulting in a manifold of $2m$ nondegenerate bound states. Among these, let us call $\delta\omega_{m,N}$ the energy gap between the pair of the most internal ones and $|\langle\hat{a}_1^\dagger\hat{a}_L\rangle|$ the absolute value of their end-to-end amplitude. Then, for $J_{\rm mod}=J_2$, $\delta\omega_{m,N}$ and $|\langle\hat{a}_1^\dagger\hat{a}_L\rangle|$ are, respectively, the same as $\delta\omega$ and the corresponding end-to-end amplitude of a staggered array of size L [see Eq. (8) and Fig. 3(a)]. In the

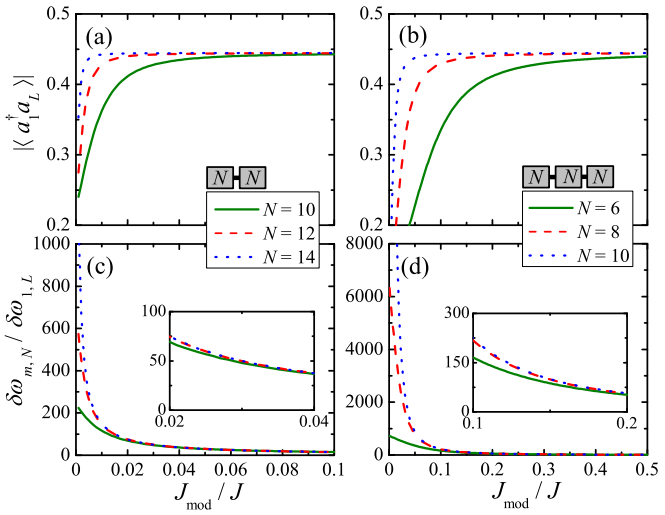

FIG. 4. Full-array end-to-end (a, b) amplitude $|\langle \hat{a}_1^\dagger \hat{a}_L \rangle|$ and (c, d) energy-gap gain $\delta\omega_{m,N}/\delta\omega_{1,L}$ vs $J_{\rm mod}/J$ for different values of N in the case of a modularized staggered CCA. (a, c) Two-module array ($m = 2$); (b, d) three-module array ($m = 3$). For each setup, we have set the intramodule distortion to $\eta = -0.5$ (about $J_1/J_2 = 0.33$).

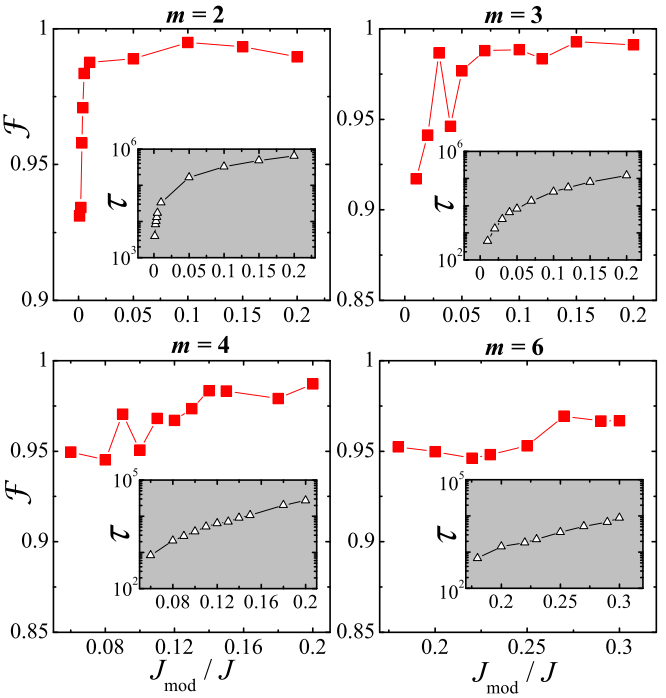

FIG. 5. Maximum achievable average QST fidelity $\mathcal{F}$ [cf. Eq. (11)] after one Rabi-like oscillation period, that is, $\tau = 2\pi/\delta\omega_{m,N}$, vs $J_{\rm mod}/J$. We have set $L = 24$, $J_1 = 0.3J$, and $J_2 = J$ and considered different modularization schemes (each specified by the value of m). Inset: Transfer time τ (in units of J^{-1}) vs $J_{\rm mod}/J$ on a log-lin scale. For the unmodularized array ($m = 1$), the maximum fidelity and transfer time are, respectively, $\mathcal{F} \simeq 0.98$ and $\tau \simeq 3 \times 10^6 J^{-1}$.

opposite limit $J_{\rm mod} = 0$, $\delta\omega_{m,N}$ is *larger*, since now it coincides with the bound-state gap of a staggered array of size $N < L$, while $|\langle \hat{a}_1^\dagger \hat{a}_L \rangle| = 0$ because the modules are now uncoupled.

To investigate the dependence of $\delta\omega_{m,N}$ and $|\langle \hat{a}_1^\dagger \hat{a}_L \rangle|$ on $J_{\rm mod}$, in Fig. 4 we consider the cases of a two- and three-module array ($\delta\omega_{m,N}$ is plotted in units of $\delta\omega_{1,L}$, namely, its value at $J_{\rm mod} = J_2$). As $J_{\rm mod}$ increases from 0, both the gap and the end-to-end amplitude monotonically tend to their respective values for $J_{\rm mod} = J_2$ (i.e., the case discussed above). Remarkably, the end-to-end amplitude, in particular, exhibits quite a rapid saturation [see Figs. 4(a) and 4(b)]. Instead, $\delta\omega_{m,N}$ undergoes more regular growth. This means that, starting from $J_{\rm mod} = J_2$ (L-size staggered array), one can decrease $J_{\rm mod}$ by a significant amount—thus modularizing the CCA—and retain the end-to-end amplitude almost unchanged, but amplifying the energy gap substantially. For instance [see Figs. 4(a) and 4(c)], in the two-module ($m = 2$) case for $N = 14$ when $J_{\rm mod} \simeq 0.01J$ the end-to-end amplitude is unchanged for all practical purposes while the energy gap is over a hundred times larger, resulting in the same QST fidelity but with a transfer time about two orders of magnitude lower. This can be further improved by increasing the number of modules for fixed overall array length L since this results in modules of a shorter length.

We also note in Fig. 4 that the saturation of $|\langle \hat{a}_1^\dagger \hat{a}_L \rangle|$ occurs for lower values of $J_{\rm mod}$ as N grows. Hence, lower values of $J_{\rm mod}$ are required for establishing bilocalization. This can be attributed to the fact that the gap $\delta\omega$ of each (isolated) staggered module, coinciding with $\delta\omega_{m,N}$ for $J_{\rm mod} = 0$, decreases with N. From a perturbative perspective, the effect of switching on an intermodular coupling will be significant when $J_{\rm mod}$ becomes comparable with $\delta\omega$, which, however, decreases with N.

To summarize, for a staggered array of a given length, partitioning it into several modules can result in shorter QST times without significantly affecting the corresponding fidelity. In Fig. 5, we provide further explicit evidence of this phenomenon by considering a CCA of length $L = 24$ in the case of four modularizations, defined by $m = 2$, 3, 4, and 6. Note, for instance, that a six-block modularization leaves the fidelity above $\simeq$95%, while the QST time is shortened by three orders of magnitude. A significant QST speedup is nevertheless attainable even for lower m. Note that while the QST time increases polynomially with $J_{\rm mod}$, the fidelity shows nonmonotonic behavior due to residual contributions from other eigenstates to the transition amplitude [see Eq. (13)].

The possibility of reducing QST times over relatively short distances—say of the order of up to 30 sites as in Fig. 5—is relevant itself, e.g., to carry out short-haul communications tasks between quantum processors in a quantum computing architecture. Concerning longer CCAs, a thorough analysis of the scalability of a modularized array is beyond the scope of the present work and will thus be presented elsewhere [60]. However, in order to test the potential of modularized chains to perform QST over longer distances, in Fig. 6 we additionally consider the paradigmatic case of a CCA having $L = 102$ sites. Note that high-quality QST is still achievable within times that, although inevitably longer, are far shorter compared to the unmodularized staggered CCA.

As mentioned previously, all the above clearly applies not only to atom-free CCAs, but also to spin chains in general (regardless of their implementation). In the following, we address CCAs coupled to atoms with the goal of putting forward QST schemes in which both atomic and photonic degrees of freedom are involved.

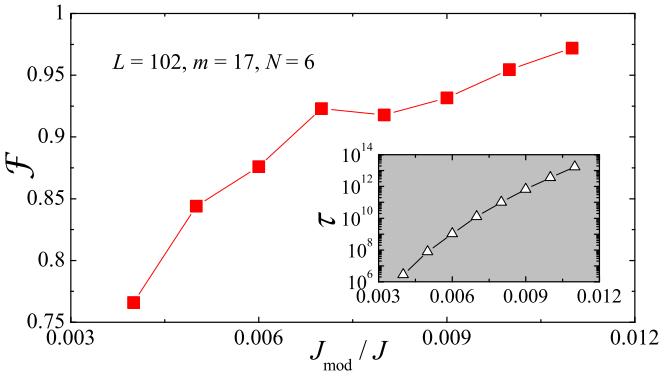

FIG. 6. Maximum achievable average QST fidelity $\mathcal{F}$ [cf. Eq. (11)] after one Rabi-like oscillation period, that is, $\tau = 2\pi/\delta\omega_{m,N}$, vs $J_{\rm mod}/J$. We have set $L = 102$ and $\eta = -0.8$ (about $J_1/J_2 = 0.11$) using the modularization scheme $m = 17$, the length of each module thus being $N = 6$. Inset: Transfer time τ (in units of J^{-1}) vs $J_{\rm mod}/J$ on a log-lin scale. For the corresponding unmodularized CCA, the transfer time is infinite for all practical purposes.

VI. CCA WITH ATOMS

We now consider a CCA where each cavity is additionally coupled to a two-level atom of frequency ω_a, according to the JC interaction Hamiltonian [61],

$$\hat{H}_x^{(\rm JC)} = \omega_c \hat{a}_x^\dagger \hat{a}_x + \omega_a \hat{\sigma}_x^+ \hat{\sigma}_x^- + g\,(\hat{\sigma}_x^+ \hat{a}_x + \hat{\sigma}_x^- \hat{a}_x^\dagger), \tag{19}$$

where now $\hat{\sigma}_x^+ \equiv |{\rm e}\rangle_x\langle{\rm g}|$, with $|{\rm g}\rangle$ ($|{\rm e}\rangle$) denoting the atomic ground (excited) state, and g the atom-field coupling strength. In the following, we again set $\omega_c = 0$ for simplicity. For a staggered pattern of hopping rates (see Fig. 1), the total Hamiltonian reads

$$\hat{H} = \hat{H}_{\rm hop} + \sum_{x=1}^{N} \hat{H}_x^{(\rm JC)}, \tag{20}$$

where the hopping Hamiltonian is the same as in Eq. (1). Hereafter, we adopt the short notation $|1_x\rangle \equiv \hat{a}_x^\dagger|{\rm vac}\rangle|{\rm g}\rangle_1 \ldots |{\rm g}\rangle_N$ and $|e_x\rangle \equiv \hat{\sigma}_x^+|{\rm vac}\rangle|{\rm g}\rangle_1 \ldots |{\rm g}\rangle_N$, where the former is the state where a single photon lies in the xth cavity with all the atoms unexcited, while in the latter state only the xth atom is excited (with the field and all of the remaining atoms unexcited). The single-excitation sector of the joint Hilbert space is $2N$-dimensional and spanned by the basis $\{|1_x\rangle, |e_x\rangle\}$.

Moreover, let us denote $\{|\alpha_n\rangle\}$ the set of N eigenstates of the free-field Hamiltonian $\hat{H}_{\rm hop}$, i.e., $\hat{H}_{\rm hop}|\alpha_n\rangle = \omega_n|\alpha_n\rangle$, each having the form $|\alpha_n\rangle = \sum_x \alpha_{nx}|1_x\rangle$. These states solely comprise photonic excitations (the index n is intended to run over both bound and unbound states). Correspondingly, one can define a set of N states $\{|\beta_n\rangle\}$ such that $|\beta_n\rangle = \sum_x \alpha_{nx}|e_x\rangle$, hence featuring only atomic excitations (excitons). By construction, each $|\beta_n\rangle$ has the same spatial profile as $|\alpha_n\rangle$ and can thus be regarded as its excitonic analog. States $\{|\alpha_n\rangle\}$ ($\{|\beta_n\rangle\}$) can be regarded as arising from the normal-mode field (atomic) operators $\{\hat{\alpha}_n\}$ ($\{\hat{\beta}_n\}$), defined, accordingly, as $\hat{\alpha}_n = \sum_x \alpha_{nx}\hat{a}_x$ ($\hat{\beta}_n = \sum_x \alpha_{nx}\hat{\sigma}_x^-$).

Note that in Eq. (20) both g and ω_a are uniform throughout the array. Using this, $\hat{H}$ can be rearranged as (see Refs. [26], [27], [29])

$$\hat{H} = \sum_n [\omega_n \hat{\alpha}_n^\dagger \hat{\alpha}_n + \omega_a \hat{\beta}_n^\dagger \hat{\beta}_n + g(\hat{\beta}_n^\dagger \hat{\alpha}_n + {\rm H.c.})]. \tag{21}$$

Therefore, within the single-excitation sector, the system behaves as a set of N *decoupled* effective JC models, each corresponding to a photonic mode of frequency ω_n coupled to its excitonic counterpart of frequency ω_a with coupling strength g. This allows for a straightforward diagonalization of $\hat{H}$ once the eigenstates of the free-field Hamiltonian $\hat{H}_{\rm hop}$, $\{|\alpha_n\rangle\}$, are known. Using the standard JC-model theory, indeed, the eigenstates are worked out as

$$|\psi_n^{(\pm)}\rangle = A_n^{(\pm)}|\alpha_n\rangle + B_n^{(\pm)}|\beta_n\rangle, \tag{22}$$

where

$$A_n^{(\pm)} = \frac{2g}{\sqrt{(\Delta_n \pm \Omega_n)^2 + 4g^2}}, \quad B_n^{(\pm)} = \frac{\Delta_n \pm \Omega_n}{\sqrt{(\Delta_n \pm \Omega_n)^2 + 4g^2}}, \tag{23}$$

with $\Delta_n = \omega_a - \omega_n$ and $\Omega_n = \sqrt{\Delta_n^2 + 4g^2}$ being the detuning and vacuum Rabi frequency, respectively, of the nth effective JC model. The corresponding energy levels read

$$\varepsilon_n^{(\pm)} = \tfrac{1}{2}(\omega_a + \omega_n \pm \Omega_n). \tag{24}$$

A. Single-mode resonance

Of all the N effective JC dynamics [cf. Eq. (21)] one can selectively excite only one of them upon a judicious tuning of the atomic frequency ω_a. Now we particularly show how to trigger only the JC dynamics corresponding to the bound eigenstate $|\alpha_{b+}\rangle$ [cf. Eq. (9)]. In the interaction picture, Hamiltonian (21) is turned into (we now highlight explicitly the contributions of the bound and unbound states)

$$\hat{H}_{\rm I}(t) = g\left[\sum_{j=\pm} \hat{\beta}_{bj}^\dagger \hat{\alpha}_{bj} e^{i\Delta_{bj}t} + \sum_{k\mu} \hat{\beta}_{k\mu}^\dagger \hat{\alpha}_{k\mu} e^{i\Delta_{k\mu}t} + {\rm H.c.}\right] \tag{25}$$

with $\Delta_{b\pm} = \omega_a - \omega_{b\pm}$ and $\Delta_{k\mu} = \omega_a - \omega_{k\mu}$. By tuning ω_a on resonance with ω_{b+}, namely, setting $\omega_a = \omega_{b+}$, the first term becomes time independent. If, additionally, $g \ll \{\Delta_{k\mu}, \Delta_{b-}\}$, all the remaining terms in Eq. (25) are rapidly rotating so that they effectively do not affect the dynamics and, hence, can be neglected. Returning to the Schrödinger picture, we thus end up with an effective Hamiltonian of the form

$$\hat{H}_{\rm eff} = \sum_n (\omega_n \hat{\alpha}_n^\dagger \hat{\alpha}_n + \omega_a \hat{\beta}_n^\dagger \hat{\beta}_n) + g(\hat{\beta}_{b+}^\dagger \hat{\alpha}_{b+} + {\rm H.c.}). \tag{26}$$

An analogous conclusion holds if we set the atomic frequency on resonance with ω_{b-}. The dynamics thus consists of a resonant JC-like dynamics involving $|\alpha_{b+}\rangle$ and its excitonic analog, while all the remaining photonic and atomic modes evolve freely. Accordingly, only the pair of dressed states $|\psi_{b+}^{(\pm)}\rangle$ is thus formed [cf. Eq. (22)]. Note that, due to the resonance condition $\Delta_{b+} = 0$, we get $|A_{b+}^{(\pm)}| = |B_{b+}^{(\pm)}|$ [cf. Eq. (23)]. Hence, $|\psi_{b+}^{(\pm)}\rangle$ are fully dressed states featuring maximal atom-photon entanglement.

B. Strong-coupling regime

Clearly, an implicit requirement for the above regime to hold is that $g \ll \delta\omega$ (since $|\alpha_{b-}\rangle$ is the nearest state in energy). If not, additional coupling terms between field modes and the respective excitonic analogues would appear in Eq. (26). Consider, in particular, the strong-coupling regime [27,32] such that g is far larger than the entire range of the field frequencies ($\omega_a = 0$, for simplicity). Then none of the coupling terms in Eq. (21) can be neglected in a way so that each corresponding JC dynamics is activated. Also, due to the negligible detunings, *all* the pairs of states in Eq. (22) are formed, each reading $|\psi_n^{(\pm)}\rangle \simeq (|\alpha_n\rangle \pm |\beta_n\rangle)/\sqrt{2}$ and, thus, embodying fully dressed states. Accordingly, the energy spectrum [cf. Eq. (24)] reduces to $\varepsilon_n^{(\pm)} \simeq \omega_n/2 \pm g$ (since $\Omega_n \simeq 2g$). Thereby, in this regime two independent polaritonic bands are formed, each corresponding to even (odd) dressed states $|\psi_n^{(+)}\rangle$ ($|\psi_n^{(-)}\rangle$). In either of these, the dynamics thus reduces to a single polariton subjected to an effective Hamiltonian that is analogous to the free-field hopping Hamiltonian, (1) [or (18) in the case of modularization] but with all the hopping rates rescaled by a factor of $1/2$. If the CCA is prepared in a state such as $(|e_1\rangle \pm |1_1\rangle)/\sqrt{2}$, then only the corresponding band will be excited and the dynamics will be the same as that analyzed in previous sections [with each single-photon state $|x\rangle$ now replaced with the single-cavity polariton state $(|e_x\rangle \pm |1_x\rangle)/\sqrt{2}$].

VII. TRANSFER OF ATOMIC AND POLARITONIC STATES

Depending on the single-mode resonance or strong-coupling regimes discussed in Secs. VI A and VI B, respectively, we now show that one can carry out transfer of an atomic or polaritonic state.

A. Atomic QST through single-mode resonance

Setting $\omega_a = \omega_{b+}$ and $g \ll \delta\omega$, the latter being the gap between the bilocalized states $|\alpha_{b\pm}\rangle$, the JCH Hamiltonian takes the effective form of Eq. (26). If the parameters entering Eq. (1) [or Eq. (18) for modularized CCAs] are such that strong bilocalization occurs (see Secs. II, IV, and V), then both the excitonic states, $|e_1\rangle$ and $|e_N\rangle$, can be decomposed to a good approximation only in terms of $|\beta_{b\pm}\rangle$. This gives $|e_1\rangle \simeq \sum_{j=\pm}\langle\beta_{bj}|e_1\rangle|\beta_{bj}\rangle$, and, using the parity properties of $|\beta_{b\pm}\rangle$, $|e_N\rangle \simeq -\langle\beta_{b-}|e_1\rangle|\beta_{b-}\rangle + \langle\beta_{b+}|e_1\rangle|\beta_{b+}\rangle$. Expressing next $|\beta_{b+}\rangle$ in terms of dressed states [see Eq. (22)], we get $|\beta_{b+}\rangle = \frac{1}{\sqrt{2}}(|\psi_{b+}^{(+)}\rangle - |\psi_{b+}^{(-)}\rangle)$, where $|\psi_{b+}^{(\pm)}\rangle$ has energy $\omega_0 \pm g$. Replacing it in the above decomposition for $|e_1\rangle$ and letting this evolve in time through to the usual time-evolution operator $\hat{U}(t)$, we get

$$\hat{U}(t)|e_1\rangle \simeq \langle\beta_{b-}|e_1\rangle|\beta_{b-}\rangle + \frac{\langle\beta_{b+}|e_1\rangle}{\sqrt{2}}(e^{-igt}|\psi_{b+}^{(+)}\rangle - e^{igt}|\psi_{b+}^{(-)}\rangle) \tag{27}$$

up to an irrelevant global phase factor. Expressing again the dressed states in terms of $|\alpha_{b+}\rangle$ and $|\beta_{b+}\rangle$,

$$\hat{U}(t)|e_1\rangle \simeq \langle\beta_{b-}|e_1\rangle|\beta_{b-}\rangle + \langle\beta_{b+}|e_1\rangle[\cos(gt)|\beta_{b+}\rangle - i\sin(gt)|\alpha_{b+}\rangle]. \tag{28}$$

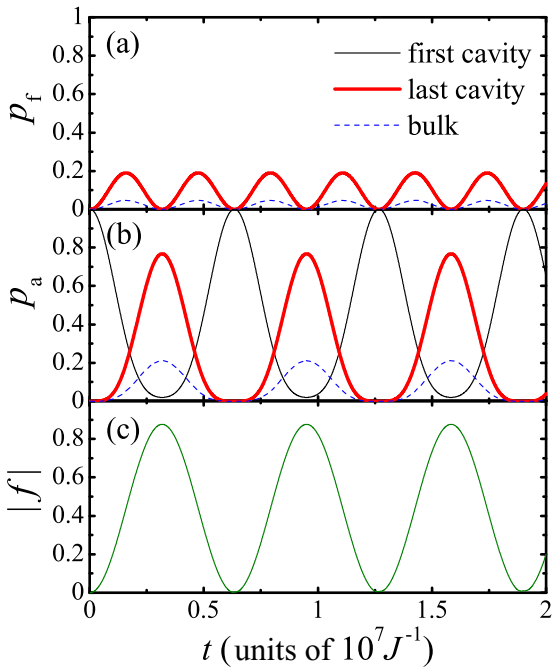

FIG. 7. Time evolution of (a) the photonic and (b) the atomic excitation and (c) of the transition amplitude across a 10-cavity staggered CCA for an initial state $|\Psi(0)\rangle = |e_1\rangle$. In (a) [(b)], we display the probability of finding the photonic [atomic] excitation in the first cavity (thin black line), in the last one (thick red line), and in the bulk sites $2 \leqslant x \leqslant N-1$ (dashed blue line). Plots were obtained from an exact numerical diagonalization of Eq. (20) for $\eta = -0.5$ and $g = 10^{-6}J$.

For $gt = \pi$ (up to an irrelevant global phase factor), we thus get (see above) $\hat{U}(t)|e_1\rangle \simeq |e_N\rangle$. Noting that, in the light of Sec. III, the state in which the CCA has zero excitations (both photonic and atomic) does not evolve, the two-level atom constitutes a natural choice for encoding the logical qubit. Therefore, a QST protocol can be carried out between the outermost atoms in a transfer time $\tau = \pi/g$. Likewise, one can accordingly define a transition amplitude (cf. Sec. III) as $f(t) = \langle e_N|\hat{U}(t)|e_1\rangle$ and evaluate the QST efficiency using Eq. (11) for the average fidelity.

In Fig. 7, we study in a paradigmatic instance (such that $|\Psi(0)\rangle = |e_1\rangle$) the time evolution of the photonic and atomic excitations alongside the transition amplitude just introduced. We denote $p_{f,x}(t) = |\langle 1_x|\Psi(t)\rangle|^2$ and $p_{a,x}(t) = |\langle e_x|\Psi(t)\rangle|^2$ the probability of finding one photon and one exciton at cavity x, respectively. As shown in Fig. 7, the transfer takes place through the involvement of the entire CCA, including the bulk (especially in the form of excitons). Note that, while the considered array is only moderately distorted (we take $\eta = -0.5$), $|f|$ attains a maximum $\simeq 0.9$.

B. Polariton transmission in the strong-coupling regime

Note that in the scheme discussed previously, the transfer time τ is in fact set by the atom-field coupling strength g, which is required to be much smaller than the energy gap between bilocalized modes $\delta\omega$. As the latter decreases with the array distortion (see Sec. II), this scheme can be demanding

for highly distorted CCAs. In this scenario, the properties of an atom-free CCA, as shown in Secs. II, IV, and V, can be exploited to transfer polaritonic states across the array.

In the strong-coupling regime (see Sec. VI B), the dynamics reduces to that of a pair of fully dressed polaritonic bands. In either of these, a single-cavity polariton of a given parity hops through the array just like a photon propagates through an atom-free CCA (see Secs. II, IV, and V) apart from a factor-of-1/2 rescaling of the hopping rates (hence half the propagation speed). Given that the polaritonic bands are uncoupled, the preparation of a polariton of a given parity in a given cavity, say $\frac{1}{\sqrt{2}}(|e_1\rangle + |1_1\rangle)$, will trigger a dynamics where solely polaritons of the same parity are involved. Hence, at least in principle, one can encode a qubit in each cavity in terms of atom-photon logical states $|\mathrm{vac}\rangle|\mathrm{g}\rangle_1 \ldots |\mathrm{g}\rangle_N$ and $\frac{1}{\sqrt{2}}(|e_x\rangle + |1_x\rangle)$. Accordingly, in this framework and by virtue of Sec. III, this leads to a transition amplitude defined as $f(t) = \frac{1}{2}(\langle e_N| + \langle 1_N|)\hat{U}(t)(|e_1\rangle + |1_1\rangle)$. Regardless of the feasibility of such a qubit implementation, $f(t)$ can be used as a figure of merit to measure how reliably a polaritonic state can be transmitted across the CCA in line with other studies [23,24,26,27].

Interestingly, in order for the polariton transfer to be effective, the requirement that g must be strong enough in order to enable the entire set of dressed states to form is not strict. Indeed, the nature of QST across an atom-free CCA investigated in Secs. II, IV, and V should make clear that, for a sufficiently distorted array, it is enough that g is strong enough to enable the formation of the four bilocalized dressed states $|\psi_{b\pm}^{(\pm)}\rangle$ only. In Fig. 8, we show how the onset of such dressing benefits polaritonic transfer, as the CCA is progressively distorted for a fixed value of the atom-field coupling strength g. For the uniform array, i.e., $\eta = 0$ [see Fig. 8(a)] the transmission has a poor efficiency. As we have set $\omega_a = 0$ (middle of the free-field spectrum), thus not matching any field normal mode, and because g is small, the evolution is dominated by its free-field dynamics. Hence, the atomic component of the initial polariton is almost frozen [27,32], while the photonic component propagates freely along the array, bouncing back and forth, with the dynamics ruled mostly by the unbound modes. The polaritonic transition amplitude significantly increases already upon the introduction of a small amount of distortion [see Fig. 8(b)]. Now, the bound bilocalized modes dominate the dynamics and the transition amplitude accordingly exhibits a periodic behavior. A small contribution from the photonic unbound states, which results in short-time beatings, is still present. Moreover, g is still not much higher than $\delta\omega$, hence the dressing of the bilocalized modes is not maximum. In Fig. 8(c), we further distort the CCA in a way that the transition amplitude reaches considerably higher values. As a consequence, the required transmission time grows since the array distortion causes the gap $\delta\omega$ to decrease. However, based on the modularization scheme introduced in Sec. V, this drawback can be gotten around. This is shown in Fig. 8(d), where we consider a CCA split into 3 (5) weakly connected modules each comprising 10 (6) cavities. Note that, compared with Fig. 8(c), the time required to complete the polaritonic-state transfer is considerably shortened, while the maximum transition amplitude is almost unaffected.

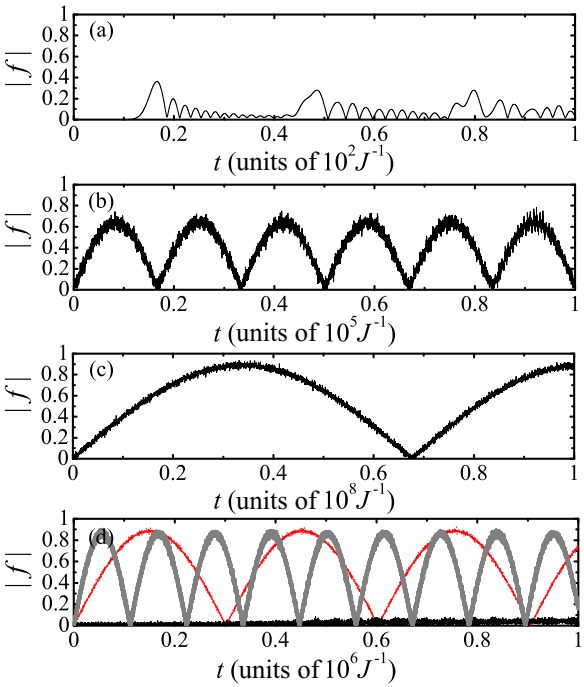

FIG. 8. Time evolution of the transition amplitude for an initial symmetric polariton set in the first cavity in the case of a staggered 30-cavity array for (a) $\eta = 0$, (b) $\eta = -0.25$, and (c) $\eta = -0.5$ (solid black line). (d) The case of a modularized CCA for $m = 3$ with $J_{\mathrm{mod}} = 0.1J$ (dotted red line) and $m = 5$ with $J_{\mathrm{mod}} = 0.3J$ (thick gray line). Note that J_{mod} was slightly increased in order to assure the formation of bilocalized states (cf. Sec. V). The intramodular distortion parameter was fixed at $\eta = -0.5$. We set $g = 0.01J$ and $\omega_a = 0$ throughout. Plots were obtained from an exact diagonalization of Eq. (20) [with $\hat{H}_{\mathrm{hop}}$ being replaced with $\hat{H}_{\mathrm{mod}}$ in (d)].

Regardless of the interaction regime (single-resonance or strong coupling), the crucial factor affecting the transfer fidelity is the end-to-end localization amplitude, i.e., the occurrence of bilocalization in the case of either the standard staggered CCA or the modularized (partitioned) one. The key ingredient is thus inducing the formation of bilocalized field normal modes and tuning the atoms on resonance with those. The QST speed, however, can be managed by setting the appropriate regime and/or modularizing the CCA as in Sec. V.

VIII. CONCLUSIONS

In this work, we have addressed the problem of faithfully transferring quantum states across a CCA. We have shown that, while a staggered pattern of hopping rates offers shorter QST times with respect to a uniform pattern, a further significant reduction in the transfer time is achievable by imposing modularization on top of the staggered pattern. The modularization scheme yields transfer times that are up to three orders of magnitude shorter with respect to an unmodularized staggered array already for 20-site CCAs, while the gain increases for longer CCAs without affecting the performance in terms of QST fidelity.

To accomplish this task, we first focused on QST through a staggered atom-free CCA. By devising a perturbative approach to diagonalize analytically the Hamiltonian for a highly distorted array, we showed that distortion induces the appearance of bound modes that are strongly bilocalized at the array edges. In line with QST schemes exploiting bilocalization, this allows for high-fidelity QST. As a distinctive property of the staggered configuration, though, the scaling behavior of the fidelity as a function of the CCA size has ideal features since, for the high-distortion scenario, the fidelity is nearly insensitive to the array length (unlike in the case of a uniform bulk with weak outermost couplings). This, however, comes at the cost of having relatively long transfer times. To get around this drawback, we devised a strategy based on an engineered modularization of the array into identical staggered subunits. We showed that in some paradigmatic instances this can result in a significant reduction in the transfer time while retaining the transfer fidelity almost unchanged. Although we focused on an atom-free CCA, those findings apply to any spin chain regardless of the way it is implemented.

We then turned to a CCA where each cavity is coupled to an atom, with the aim of exploring how the previous outcomes can be harnessed to transfer atomic or polaritonic states between the two array ends. In the weak-coupling regime where the atomic frequency is resonant with one of the two bilocalized field modes, QST of atomic states can be achieved in a time set by the atom-field coupling strength. For stronger atom-photon couplings, one can instead exploit the formation of pairs of bilocalized dressed states to efficiently transfer a polariton of a given parity across the CCA in a time set by the energy gap between the pair of field bilocalized modes.

ACKNOWLEDGMENTS

Fruitful discussions with D. L. Feder, S. Lorenzo, and G. M. Palma are acknowledged. This work was supported by CNPq. T.J.G.A. acknowledges the EU Collaborative Project TherMiQ (Grant No. 618074). F.C. acknowledges support from Italian PRIN-MIUR 2010/2011MIUR (PRIN 2010-2011).

[1] M. J. Hartmann, F. G. S. L. Brandão, and M. B. Plenio, Laser Photon. Rev. **2**, 527 (2008).
[2] A. Tomadin and R. Fazio, J. Opt. Soc. Am. B **27**, A130 (2010).
[3] D. G. Angelakis, M. F. Santos, and S. Bose, Phys. Rev. A **76**, 031805(R) (2007).
[4] A. D. Greentree, C. Tahan, J. H. Cole, and L. C. L. Hollenberg, Nat. Phys. **2**, 856 (2006).
[5] M. J. Hartmann, F. G. S. L. Brandão, and M. B. Plenio, Nat. Phys. **2**, 849 (2006).
[6] D. Rossini and R. Fazio, Phys. Rev. Lett. **99**, 186401 (2007).
[7] M. Aichhorn, M. Hohenadler, C. Tahan, and P. B. Littlewood, Phys. Rev. Lett. **100**, 216401 (2008).
[8] J. Koch and K. Le Hur, Phys. Rev. A **80**, 023811 (2009).
[9] S. Schmidt and G. Blatter, Phys. Rev. Lett. **103**, 086403 (2009).
[10] P. Pippan, H. G. Evertz, and M. Hohenadler, Phys. Rev. A **80**, 033612 (2009).
[11] S. Schmidt and G. Blatter, Phys. Rev. Lett. **104**, 216402 (2010).
[12] M. Knap, E. Arrigoni, and W. von der Linden, Phys. Rev. B **81**, 104303 (2010).
[13] K. M. Birnbaum, A. Boca, R. Miller, A. D. Boozer, T. E. Northup, and H. J. Kimble, Nature **436**, 87 (2005).
[14] M. P. A. Fisher, P. B. Weichman, G. Grinstein, and D. S. Fisher, Phys. Rev. B **40**, 546 (1989).
[15] J. Raftery, D. Sadri, S. Schmidt, H. E. Türeci, and A. A. Houck, Phys. Rev. X **4**, 031043 (2014).
[16] H. J. Kimble, Nature **453**, 1023 (2008).
[17] J. I. Cirac, P. Zoller, H. J. Kimble, and H. Mabuchi, Phys. Rev. Lett. **78**, 3221 (1997).
[18] A. Serafini, S. Mancini, and S. Bose, Phys. Rev. Lett. **96**, 010503 (2006).
[19] T. Chanelière, D. N. Matsukevich, S. D. Jenkins, S.-Y. Lan, T. A. B. Kennedy, and A. Kuzmich, Nature **438**, 833 (2005).
[20] S. Ritter, C. Nölleke, C. Hahn, A. Reiserer, A. Neuzner, M. Uphoff, M. Mücke, E. Figueroa, J. Bochmann, and G. Rempe, Nature **484**, 195 (2012).
[21] S. Bose, Phys. Rev. Lett. **91**, 207901 (2003).
[22] T. J. G. Apollaro, S. Lorenzo, and F. Plastina, Int. J. Mod. Phys. B **27**, 1345035 (2013).
[23] F. K. Nohama and J. A. Roversi, J. Mod. Opt. **54**, 1139 (2007).
[24] S. Bose, D. G. Angelakis, and D. Burgarth, J. Mod. Opt. **54**, 2307 (2007).
[25] F. M. Hu, L. Zhou, T. Shi, and C. P. Sun, Phys. Rev. A **76**, 013819 (2007).
[26] C. D. Ogden, E. K. Irish, and M. S. Kim, Phys. Rev. A **78**, 063805 (2008).
[27] M. I. Makin, J. H. Cole, C. D. Hill, A. D. Greentree, and L. C. L. Hollenberg, Phys. Rev. A **80**, 043842 (2009).
[28] J. Lu, L. Zhou, H. C. Fu, and L.-M. Kuang, Phys. Rev. A **81**, 062111 (2010).
[29] F. Ciccarello, Phys. Rev. A **83**, 043802 (2011).
[30] Y.-L. Dong, S.-Q. Zhu, and W.-L. You, Phys. Rev. A **85**, 023833 (2012).
[31] G. Dong, Y. Zhang, M. Arshad Kamran, and B. Zou, J. Appl. Phys. **113**, 143105 (2013).
[32] G. M. A. Almeida and A. M. C. Souza, Phys. Rev. A **87**, 033804 (2013).
[33] J. Q. Quach, Phys. Rev. A **88**, 053843 (2013).
[34] L. Latmiral, C. Di Franco, P. L. Mennea, and M. S. Kim, Phys. Rev. A **92**, 022350 (2015).
[35] N. Behzadi, S. K. Rudsary, and B. A. Salmas, Eur. Phys. J. D **67**, 247 (2013).
[36] L. Zhou, Z. R. Gong, Y.-x. Liu, C. P. Sun, and F. Nori, Phys. Rev. Lett. **101**, 100501 (2008).
[37] P. Longo, P. Schmitteckert, and K. Busch, Phys. Rev. Lett. **104**, 023602 (2010).
[38] M. Biondi, S. Schmidt, G. Blatter, and H. E. Türeci, Phys. Rev. A **89**, 025801 (2014).
[39] S. Felicetti, G. Romero, D. Rossini, R. Fazio, and E. Solano, Phys. Rev. A **89**, 013853 (2014).
[40] F. Lombardo, F. Ciccarello, and G. M. Palma, Phys. Rev. A **89**, 053826 (2014).

[41] T. G. Tiecke, J. D. Thompson, N. P. de Leon, L. R. Liu, V. Vuletić, and M. D. Lukin, Nature **508**, 241 (2014).
[42] M. Christandl, N. Datta, A. Ekert, and A. J. Landahl, Phys. Rev. Lett. **92**, 187902 (2004).
[43] C. Di Franco, M. Paternostro, and M. S. Kim, Phys. Rev. Lett. **101**, 230502 (2008).
[44] T. J. G. Apollaro, L. Banchi, A. Cuccoli, R. Vaia, and P. Verrucchi, Phys. Rev. A **85**, 052319 (2012).
[45] A. Zwick, G. A. Álvarez, J. Stolze, and O. Osenda, Phys. Rev. A **85**, 012318 (2012).
[46] A. Wójcik, T. Łuczak, P. Kurzyński, A. Grudka, T. Gdala, and M. Bednarska, Phys. Rev. A **72**, 034303 (2005).
[47] L. Campos Venuti, C. Degli Esposti Boschi, and M. Roncaglia, Phys. Rev. Lett. **99**, 060401 (2007).
[48] F. Plastina and T. J. G. Apollaro, Phys. Rev. Lett. **99**, 177210 (2007).
[49] S. Lorenzo, T. J. G. Apollaro, A. Sindona, and F. Plastina, Phys. Rev. A **87**, 042313 (2013).
[50] S. Paganelli, S. Lorenzo, T. J. G. Apollaro, F. Plastina, and G. L. Giorgi, Phys. Rev. A **87**, 062309 (2013).
[51] R. E. Peierls, *Quantum Theory of Solids* (Oxford University Press, New York, 1955).
[52] M. X. Huo, Y. Li, Z. Song, and C. P. Sun, Europhys. Lett. **84**, 30004 (2008).
[53] E. I. Kuznetsova and A. I. Zenchuk, Phys. Lett. A **372**, 6134 (2008).
[54] L. Campos Venuti, S. M. Giampaolo, F. Illuminati, and P. Zanardi, Phys. Rev. A **76**, 052328 (2007).
[55] S. M. Giampaolo and F. Illuminati, Phys. Rev. A **80**, 050301 (2009).
[56] S. M. Giampaolo and F. Illuminati, New J. Phys. **12**, 025019 (2010).
[57] S. Lorenzo, T. J. G. Apollaro, S. Paganelli, G. M. Palma, and F. Plastina, Phys. Rev. A **91**, 042321 (2015).
[58] T. Linneweber, J. Stolze, and G. S. Uhrig, Int. J. Quantum. Info. **10**, 1250029 (2012).
[59] G. Gualdi, S. M. Giampaolo, and F. Illuminati, Phys. Rev. Lett. **106**, 050501 (2011).
[60] G. M. A. Almeida, F. Ciccarello, T. J. G. Apollaro, and A. M. C. Souza (unpublished) (2016).
[61] E. T. Jaynes and F. W. Cummings, Proc. IEEE **51**, 89 (1963).